

Supporting Information

A monovacant heteropolytungstate-incorporated trimeric carbonyl rhenium cluster, $[(\text{AsW}_{11}\text{O}_{39})\{\text{Re}(\text{CO})_3\}_3(\mu_3\text{-OH})(\mu_2\text{-OH})]^{6-}$: synthesis, structure and catalytic property

Yanhui Zhang, Dongdi Zhang, Zhiyuan Huo, Pengtao Ma, Jingping Wang and
Jingyang Niu*

Section S1. Synthesis and General characterization

1-1. Synthesis of $\text{C}_{88}\text{H}_{221}\text{As}_4\text{N}_{13}\text{O}_{223}\text{Re}_{12}\text{W}_{44}$

1-2. General characterization

1-3. Single crystal X-Ray diffraction

Section S2. Basic Property Representation

2-1. Bond valence sum calculations

2-2. XRPD patterns

2-3. IR spectroscopy

2-4. UV–vis diffuse-reflectance spectroscopy and Electrochemistry properties

2-5. Thermogravimetric analysis

Section S3. Catalysis Analysis

3-1. Catalysis Analysis of (Table 1, entry 5)

Section S4. References

1-1. Synthesis of $C_{88}H_{221}As_4N_{13}O_{223}Re_{12}W_{44}$:

The precursor $[(CH_3)_4N]_8[HASW_9O_{34}] \cdot 11H_2O$ was synthesized as previously described.^{S1} All other chemicals were used as purchased without purification. Crystallography sample of compound **1** was synthesized by conventional step-by-step method.

Compound **1**: $Re(CO)_5Cl$ (0.09 g, 0.250 mmol) in 3 mL CH_3CN was dissolved at 65 °C in the dark for 0.5 h (**A**). $[(CH_3)_4N]_8[HASW_9O_{34}] \cdot 11H_2O$ (0.3 g, 0.109 mmol) was dissolved in 20mL distilled water (at this point the pH was 5.15) and boiled for 10 minutes, cooled to room temperature(**B**), then solution **A** was added dropwise into **B**, the mixture solution was heated at 80 °C for 1 h, red clear liquid was observed. Additional $[(CH_3)_4N]_8[HASW_9O_{34}] \cdot 11H_2O$ (0.1 g, 0.035 mmol) and $(CH_3)_4NCl$ (0.11 g, 1.0 mmol) were added in, then cooled and filtrated. The filtrate was allowed to stand at room temperature in the dark for slow evaporation. Red block crystals of **1** were isolated after three weeks. (Yield: 14.65 % based on $Re(CO)_5Cl$). EA and ICP calcd. (%) for $C_{88}H_{221}As_4N_{13}O_{223}Re_{12}W_{44}$ (15653.15 g·mol⁻¹): C, 6.81; H, 1.34; N 1.17, As, 1.93; W, 52.57; Re, 14.39. found: C, 6.75; H, 1.38; N, 1.19; As, 1.96; W, 53.24; Re, 14.85. IR (KBr): $\nu = 3458(\text{br, s}), 3037(\text{w}), 2023(\text{vs}), 2005(\text{vs}), 1879(\text{vs}), 1629(\text{w}), 1485(\text{s}), 956(\text{s}), 881(\text{vs}), 823(\text{s}), 793(\text{vs}), 730(\text{s}) \text{ cm}^{-1}$.

1-2. General characterization:

X-ray powder diffraction (XRPD) were performed on a Philips X' Pert-MPD instrument with Cu K α radiation ($\lambda = 1.54056 \text{ \AA}$) at room temperature. The 2θ range was 5 – 45 ° with a step size of 0.02 ° and a fixed counting time of 1 s/step. Elemental analyses (C, H and N) were conducted on a Perkin-Elmer 2400-II CHNS/O analyzer. Infrared (IR) spectroscopy was obtained from a solid sample pelletized on a Bruker VERTEX 70 IR spectrometer using KBr in the range of 400 – 4000 cm^{-1} . Thermogravimetric analysis (TGA) was carried out on a Mettler-Toledo TGA/SDTA 851^e thermobalance under a N_2 atmosphere; the temperature was ramped from 25 to 600 °C at a rate of 10 °C·min⁻¹. The electrochemical behaviors were measured on the CorrTest CS-150 analyzer (Wuhan) using saturated calomel electrode (SCE) as reference electrode. All electrochemical measurements were performed at room temperature in a standard three-electrode cell connected to a LK98 microcomputer-based electrochemical system (LANLIKE, Henan, China). Platinized carbon electrode (3 mm diameter) was used as a working electrode, a platinum wire served as the counter electrode and a mercurous chloride electrode as the reference electrode. The solutions were 10⁻⁴ M of **1** in CH_3CN – Na_2SO_4 (0.4 mol·L⁻¹) (1:3, volume ratio) and the electrochemical experiments were performed in the dark. The UV–Vis–NIR optical diffuse reflectance spectrum was measured at room temperature with a Hitachi U-4100 spectrophotometer. Data were measured in the mixed solvent CH_3CN –

H₂O (1:3, volume ratio) in the wavelength range 200–500 nm.

1-3. Single crystal X-Ray diffraction:

A red block crystal of **1** (dimensions 0.43 mm × 0.36 mm × 0.19 mm) was selected and airproofed into a glass tube. X-ray diffraction intensity data were measured on an Agilent Technologies diffract meter using supernova Mo K α radiation ($\lambda = 0.7107$ Å) at 120 K. The structure was solved by direct methods and refined using full-matrix least squares on F². All calculations were performed using the SHELXTL-97 program package^{S2} Routine Lorentz and polarization corrections were applied. The absorption correction was based on multiple and symmetry-equivalent reflections in the data set by using the SADABS program^{S3}. All hydrogen atoms were refined isotropically as a riding mode using the default SHELXTL parameters. No hydrogen atoms associated with the molecules were located from the difference Fourier map. All non-hydrogen atoms were refined anisotropically except for some water molecules. A summary of crystal data and structure refinements are listed in Table S1.

Table S1. Crystal data and structure refinement for **1**

Empirical formula	C ₈₈ H ₂₂₁ As ₄ N ₁₃ O ₂₂₃ Re ₁₂ W ₄₄
Formula weight	15653.15
Temperature	124.8(3) K
Crystal system	Tetragonal
space group	<i>P</i> -42(1) <i>c</i>
<i>a</i> /Å	23.4276(4)
<i>b</i> /Å	23.4276(4)
<i>c</i> /Å	32.0967(9)
Volume/Å ³	17616.4(7)
Z	2
Calculated density/g·cm ⁻³	2.927
μ /mm ⁻¹	18.856
F(000)	13684
Crystal size	0.43 × 0.36 × 0.19 mm
Theta range for data collection	3.03 to 25.00°
Limiting indices	-20 ≤ <i>h</i> ≤ 27, -24 ≤ <i>k</i> ≤ 27, -36 ≤ <i>l</i> ≤ 38
Reflections collected	37079
Independent reflections	13383 [R(int) = 0.0810]
Completeness to theta = 25.00	99.6%
Data / restraints / parameters	13383 / 241 / 842
Goodness-of-fit on F ²	1.053
Final R indices [I > 2σ(I)]	R1 = 0.0665, wR2 = 0.1355
R indices (all data)	R1 = 0.1079, wR2 = 0.1572
Largest diff. peak and hole/e·Å ⁻³	1.964, -1.707
Absolute structure parameter	0.00(5)

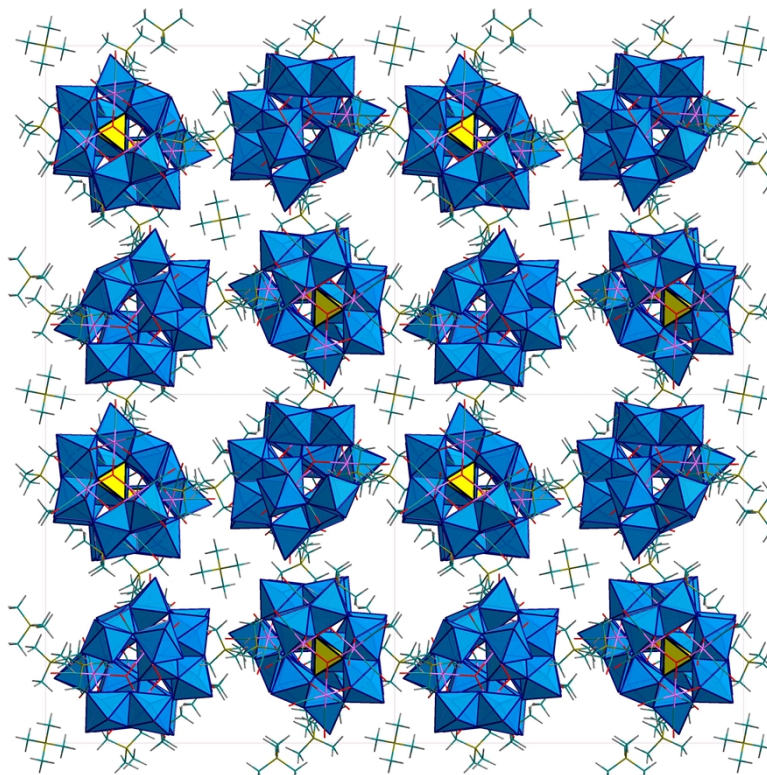


Fig. S1. The polyhedra representation of **1** along the *c* axis direction. Hydrogen atoms and H₂O molecules are omitted for clarity.

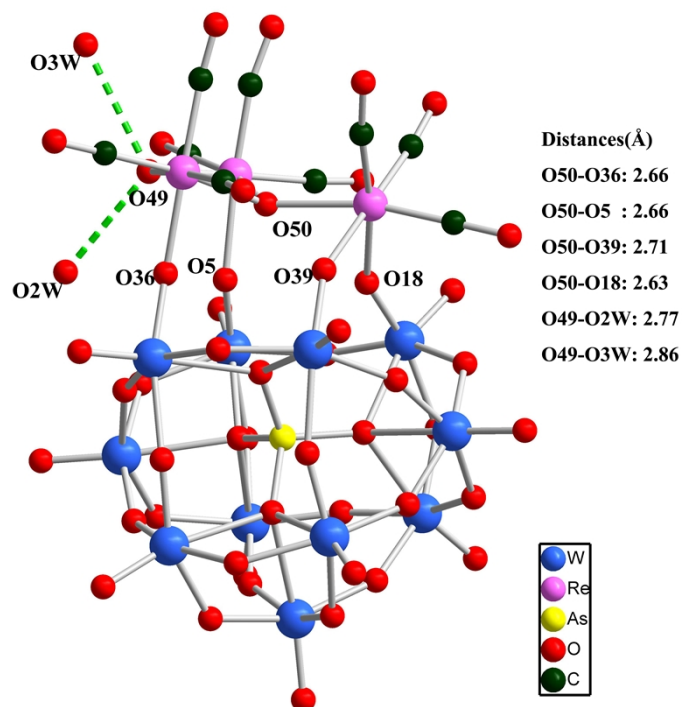


Fig. S2. The ball and stick representation of **1a** with selected labeled bonds.

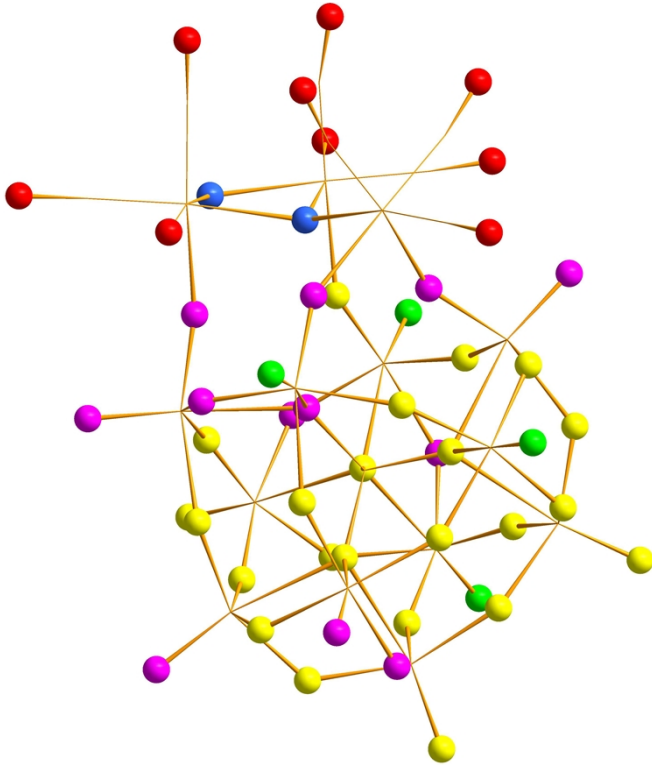
Table S2. The bond distances of Re–C and Re–O bonds of **1**. The average bond length of activated Re–C bonds is




1.93 Å, which is 0.073 Å longer than other Re–C bonds (mean values: Re–C 1.857 Å).

Bond	Length(Å)	Bond	Length(Å)	Bond	Length(Å)
Re(1)–C(3)	1.84(3)	Re(1)–C(2)	1.91(5)	Re(1)–C(1)	1.894(10)
Re(2)–C(4)	1.893(10)	Re(2)–C(5)	1.80(4)	Re(2)–C(6)	1.87(3)
Re(3)–C(7)	1.90(3)	Re(3)–C(8)	1.98(4)	Re(3)–C(9)	1.84(3)
Bond	Length(Å)	Bond	Length(Å)	Bond	Length(Å)
Re(1)–O(5)	2.11(2)	Re(1)–O(49)	2.13(2)	Re(1)–O(50)	2.147(17)
Re(2)–O(18)	2.05(2)	Re(2)–O(39)	2.09(2)	Re(2)–O(50)	2.219(17)
Re(3)–O(36)	2.072(19)	Re(3)–O(49)	2.11(2)	Re(3)–O(50)	2.196(19)

2-1. Bond valence calculations

The BVS values for different atoms in **1a** are presented in [Table S3–4](#). These values confirm that all the W atoms and As atom are in the +6 and +5 oxidation states, respectively. Furthermore, the BVS calculations of all the oxygen atoms in **1a** indicate that μ_2 -O49 and μ_3 -O50 are hydroxyl oxygen atoms.^{S4–6}



Oxygen Atom	Bong Valence sum range	Number
	-2.3 – -2.0	22
	-2.0 – -1.7	12
	-1.7 – -1.4	4

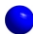

	-1.4 – -1.0	2
	Nine O atoms in carbonyl fragment of 1a	

Fig. S3. Table. S3. Charge distribution of oxygen atoms in the polyoxoanion. Oxygen atoms with different bond valence sums are represented by different colours.

Table S4. The bond valence sum calculations of W atoms and As atom in **1a**.

Atom lable	Calc. For W(VI)
W(1)	6.02
W(2)	6.70
W(3)	6.28
W(4)	6.20
W(5)	6.76
W(6)	6.08
W(7)	6.25
W(8)	6.52
W(9)	6.44
W(10)	6.24
W(11)	5.83
Atom lable	Calc. For As(V)
As(1)	4.98

2-2. XRPD patterns

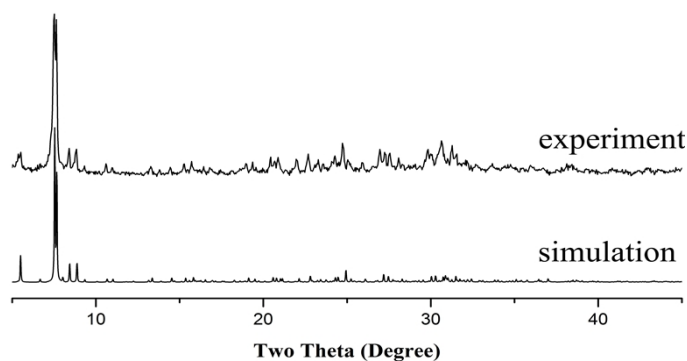


Fig. S4. Comparison of the experimental and simulated XRPD patterns of **1** in the angular range $2\theta = 5 - 45^\circ$ at 293 K.

2-3. IR spectroscopy

The FTIR spectra of **1** displays strong absorption bands at 961, 882, 826, 792, 728, 687 cm^{-1} attributed to the characteristic stretching vibration fashion of $[\alpha\text{-AsW}_{11}\text{O}_{39}]^{7-}$ containing species^{S7,S8}. Furthermore, the strong bands at (2023, 2005, 1879 cm^{-1}) assigned to two asymmetric and one symmetric stretching vibration of the CO group coordinating to the unusual $[(\text{Re}(\text{CO})_3)_3(\mu_3\text{-OH})(\mu\text{-OH})]^+$ subunit. Similar bands are observed for a number of C_{3v} carbonyl metal complexes in the carbonyl stretching region^{S9}. Comparing with IR spectra of $\text{Re}(\text{CO})_5\text{Cl}$ and

compound **1**, since the spatial location symmetric of carbonyl unit, the position of C–O stretching vibrations didn't remove obviously, while the waves number reduced and the wave strength increased intensity. Moreover, the resonance at about 3437 cm^{-1} for **1** is attributed to –OH and –NH stretching vibration and the flexural vibrations waves of –OH and –NH at 1621 and 1485 cm^{-1} are observed meanwhile. On the whole, the comparison suggests that water molecules and NH_4^+ were contained in the units. This inference is in good agreement with the results of X-ray diffraction structural analysis.

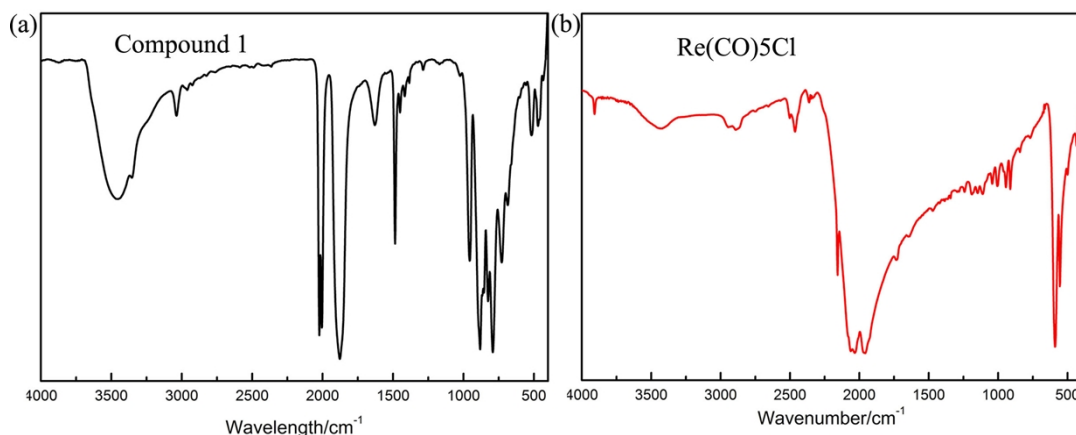


Fig. S5. IR Spectra of **1** (a) and $\text{Re}(\text{CO})_5\text{Cl}$ (b).

2-4. UV–vis diffuse-reflectance spectroscopy and Electrochemistry properties

In order to investigate the properties of **1** in the mixed solvent $\text{CH}_3\text{CN-H}_2\text{O}$ (1:3, volume ratio), the UV–vis spectra are monitored. The study of UV–vis of **1** are measured in the range of 200–500 nm, the band at about 251 nm can be attributed to the charge transfer transition $\text{O}_{2p} \rightarrow \text{W}_{5d}$ suggesting the presences of the Keggin polyoxoanions (Fig. S6).^{S10} While the absorption band at 311 nm is assigned to $\text{Re}(\text{d}\pi) \rightarrow \text{CO}(\pi^*)$ charge transition (Fig. S6, red line). On the basis of previous studies, the broad absorption band of **1** in the high visible region is likely belonging to charge-transfer of Re centers to POM ligand.

In order to investigate the stability of **1** in solution, systematic studies of UV–vis spectra and CV curves for time-dependent and pH variable in the mixed solvent were monitored (Fig. S7-10). As shown in Fig.S7–S8, compound **1** remains stable for at least 7 h at room temperature in the dark environment. On the other hand, with reducing the pH value, waves at the negative direction change strikingly when the pH is lower than 4.16. Conversely, with increasing the pH value, the peak potentials of **1** shift toward the negative direction when pH is higher than 9.65 which probably indicts that the $\{\text{Re}_3\}$ cluster separated from POM model. Meanwhile, the absorbance band at 200 nm of **1** shifted slightly when the pH values are lower than 4.63 or higher than 10.0. The

above analyses indicate that **1** is stable relatively between the pH value of 4.2 and 9.6 in the mixed solution (Fig. S9-10).

Cyclic voltammetry measurements of **1** are carried out in the mixed solvent of CH₃CN–Na₂SO₄ (0.4 mol·L⁻¹) (1:3, vol). The electrochemical behaviors are investigated in the potential range of +1.4 to –1.4 V, two pairs of closely spaced reversible and two irreversible redox waves results were exhibited for the cooperation of the redox process of the W^{VI} atoms and [Re(CO)₃]⁺ pendants. (Fig. S11a).^{S11,12} The CVs of **1** show two redox pair (II/II') at E_{1/2} = –0.616 V and another peak (III/III') at –0.803V, which corresponds to the redox processes of W^{VI} centers.^{S11} The oxidation peak (I) located at +0.959 V is attributed to the oxidation of Re(I).^{S12} Below 300 mv·s⁻¹, the peak currents are proportional to the root of the scan rates (Fig. S11b), indicating that the redox processes are probably surface-controlled.

Interestingly, POMs are a kind of appropriate catalyst candidates because they are able to deliver electrons to other species and thus served as powerful electron reservoirs for multi-electron reduction.^{S13, 14} Therefore, the electrocatalytic behavior of NO₂⁻ and H₂O₂ are taken out (Fig. S12-S13). Obviously, there is an irreversible oxidation peak that appears at the positive potential region as the nitrite is added. The parallel CVs of the CH₃CN–Na₂SO₄ (0.4 mol·L⁻¹) solution containing 0.0–0.5 mM NaNO₂ in the absence of **1** have been done, and this peak is confirmed to be NO₂⁻. The reduction peak and corresponding oxidation peak currents of W centers in the negative direction increase dramatically with stepwise addition of nitrite which exhibit well electrocatalytic activity, as well as H₂O₂.

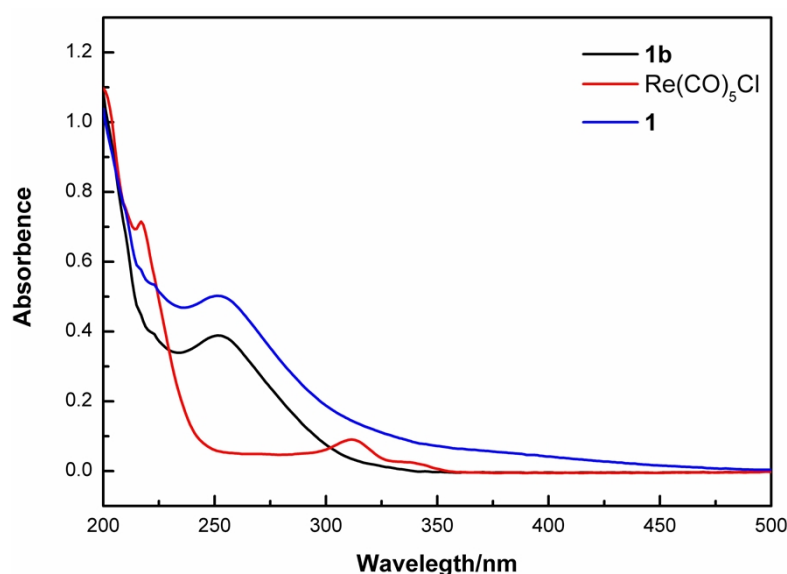


Fig. S6. Precursor **1b** (black line), Re(CO)₅Cl (red line) and compound **1** (blue line) in the mix solvent of CH₃CN–

H₂O (1:3, volume ratio).

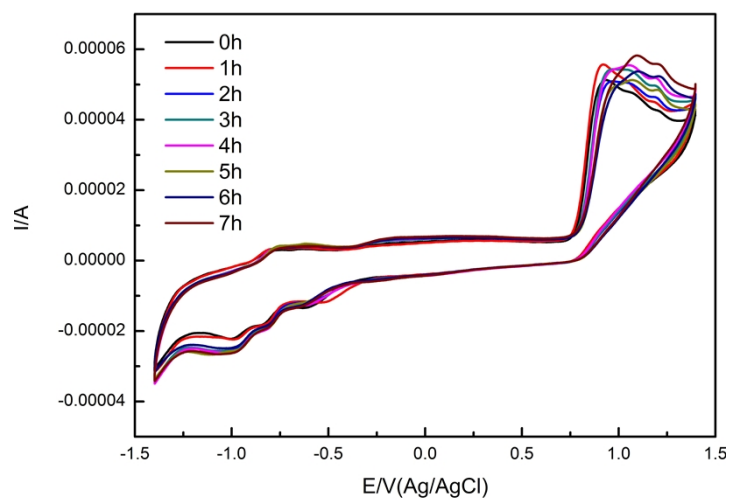


Fig. S7. The aging of the solution of **1** detected by the CV curves in the mixed solvent of CH₃CN–Na₂SO₄ (0.4 mol·L⁻¹) (1:3, volume ratio).

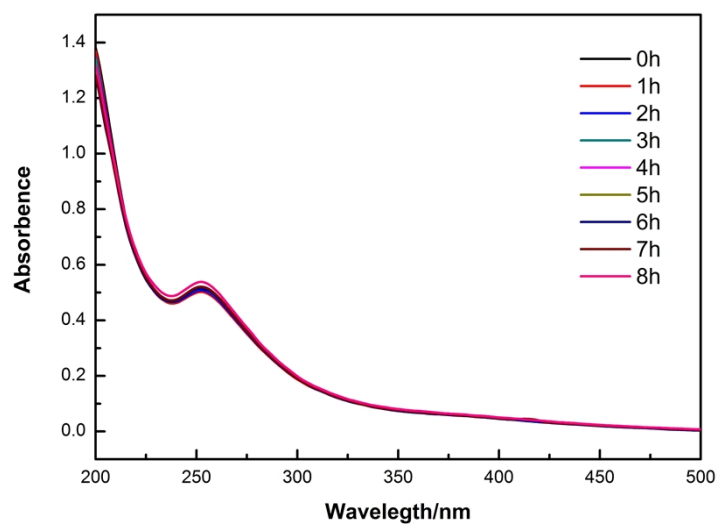


Fig. S8. The aging of the solution of **1** detected by the UV-vis spectra in the mix solvent of CH₃CN–H₂O (1:3, volume ratio).

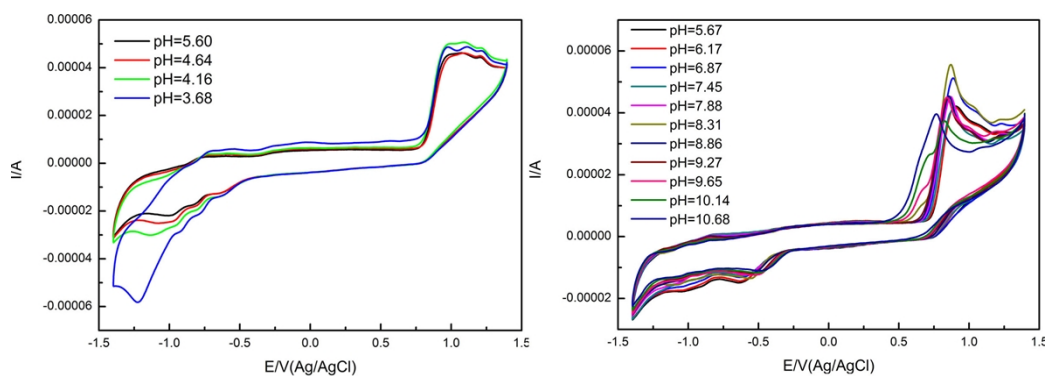


Fig. S9. The CV curves evolution of **1** in the acidic direction (left); The CV curves evolution of **1** in the alkaline

direction (right). The initial pH value of **1** dissolved in the mixed solvent of $\text{CH}_3\text{CN}-\text{Na}_2\text{SO}_4$ ($0.4 \text{ mol}\cdot\text{L}^{-1}$) (1:2, volume ratio) is 5.67. Scan rate: $100 \text{ mV}\cdot\text{s}^{-1}$. The working electrode is glassy carbon and the reference electrode is SCE. The pH values are adjusted using diluted HCl or NaOH solution.

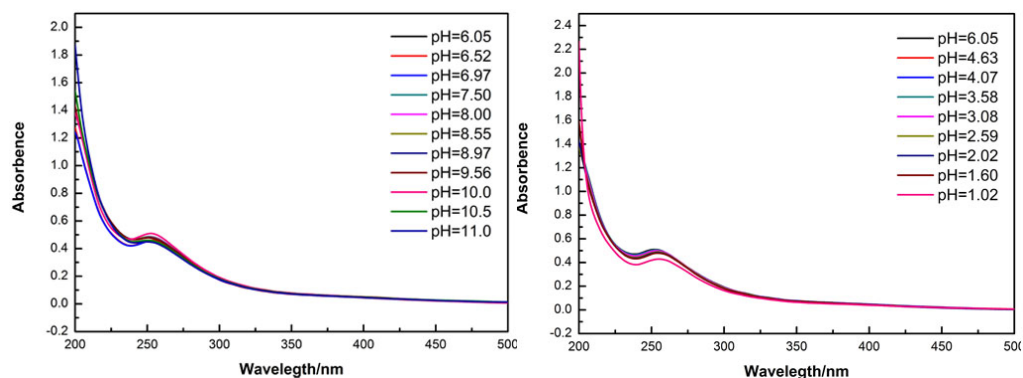


Fig. S10. The UV-vis spectra evolution of **1** in the alkaline direction (left); the UV-vis spectra evolution of **1** in the acidic direction (right).

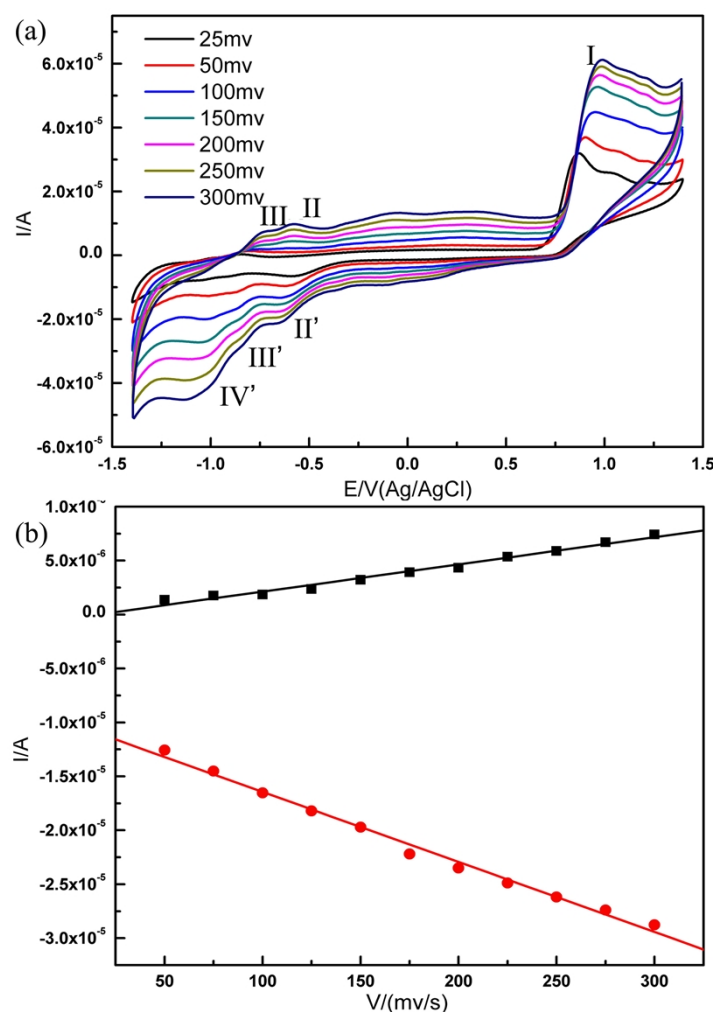


Fig. S11. (a) The CV curves of **1** in the mixed solvent of $\text{CH}_3\text{CN}-\text{Na}_2\text{SO}_4$ ($0.4 \text{ mol}\cdot\text{L}^{-1}$) (1: 3, volume ratio) at

different scan rates (from inner to outer: 20, 50, 100, 150, 200, 250, 300 $\text{mV}\cdot\text{s}^{-1}$); (b) the variation of the third couple peak currents against the square root of the scan rates from 50 to 300 $\text{mV}\cdot\text{s}^{-1}$ of **1**. The working electrode is glassy carbon and the reference electrode is SCE.

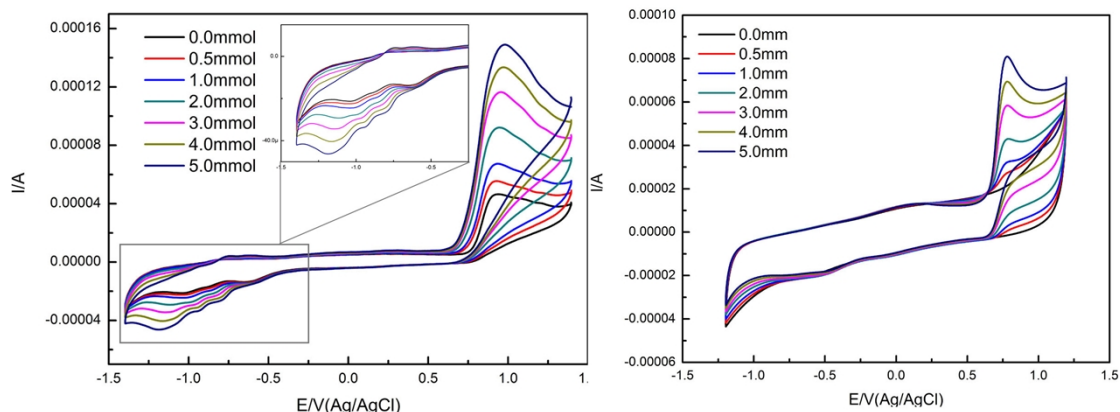


Fig. S12. The CVs of **1** in the concentration of $1\times 10^{-4} \text{ mol}\cdot\text{L}^{-1}$ at a scan rate of $100 \text{ mV}\cdot\text{s}^{-1}$ with different concentrations of NaNO_2 (left) and the CVs of absent **1** containing 0.0–5.0 mM NaNO_2 (right). Scan rate: $100 \text{ mV}\cdot\text{s}^{-1}$. The working electrode is glassy carbon and the reference electrode is SCE.

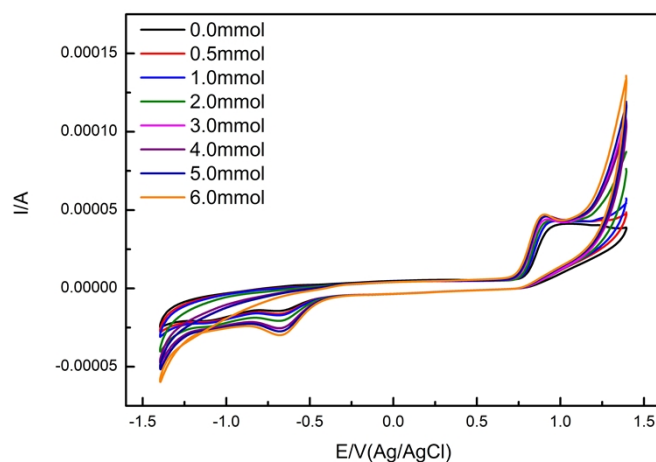


Fig. S13. The CVs of **1** in the concentration of $1\times 10^{-4} \text{ mol}\cdot\text{L}^{-1}$ with different concentrations of H_2O_2 . Scan rate: $100 \text{ mV}\cdot\text{s}^{-1}$.

2-4. Thermogravimetric analysis

To examine the thermal stability of **1**, thermal gravimetric analysis (TGA) was implemented under a N_2 atmosphere. The TG curve of **1** can be regarded as three-step of weightloss processes, giving a total loss of 19.78 % (calcd 18.89 %) in the range of 25–600 $^{\circ}\text{C}$. The first stage from 25–330 $^{\circ}\text{C}$ is ascribed to the loss of twenty-three lattice water molecules, and the observed weight loss 2.60 % is consistent with the calculated value 2.67 %. The

second stage with the weight loss of 17.18 % occurs between 330 and 600 °C, which may be attributed to the removal of thirty six carbonyl units, thirteen tetramethyl-ammonium cations and nineteen protons (in the form of constitution water molecules), and the sublimate of two As_2O_3 (calcd 16.22 %). In the high temperature region, with the POMs structure decomposed, only left the rhenium oxide and WO_3 solid finally (Fig. S14).

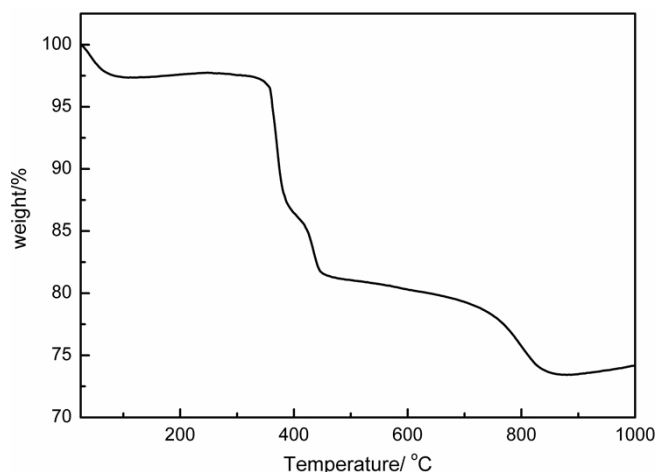
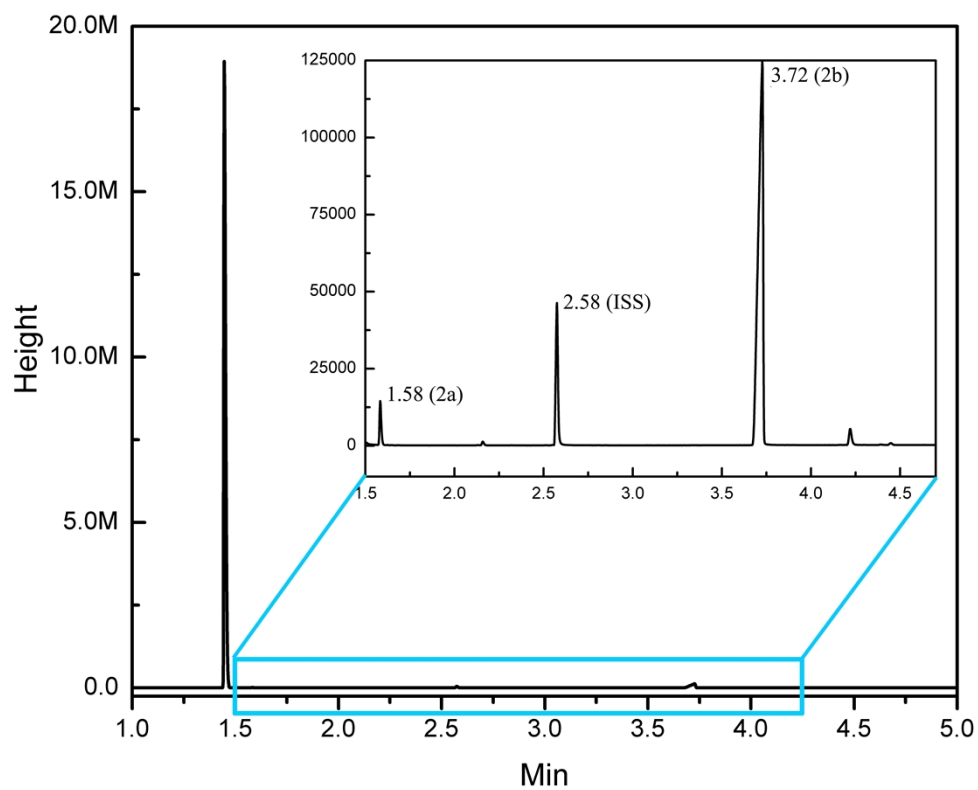


Fig. S14. The TG curve of **1**.

3-1. Catalysis Analysis

(Table 1, entry 5): epoxy chloropropane **2a** (5.0 mmol) and **cat.1** (1 μmol) are charged in a 25 mL autoclave, and then CO_2 is introduced at an initial pressure of 5.0 Mpa at room temperature. The autoclave was heated at 110 °C with stirring for 24 h. After the autoclave is cooled to room temperature, CO_2 is released slowly. To the reaction mixture, 2.0 mmol of propylene carbonate as an internal standard substance (ISS) for GC analysis is added with stirring. Ethyl acetate is used as organic solvent which appeared at 1.45 min. Analysis of the resulting mixture by GC revealed that the conversion of **2a** is 86.1 % (Fig. S15).



Study on the cycloaddition of CO₂ to chloromethyloxirane **2a** in the optimum condition: **2a**, 5 mmol; **cat.1**, 1 μ mol (0.2 mol %); CO₂, 5.0 MPa; 110 $^{\circ}$ C, 24 h. Yield: 86.1 %.

Min	Hight	Area
1.58	14400.6	172.0
2.58	46164.4	665.0
3.72	125032.1	3819.4

Fig. S15 Catalyze results for 0.5 mol % of **cat.1** (Table1, entry 5).

Section S5. References

- S1** Bi, L. H.; Huang, R. D.; Peng, J.; Wang, E. B.; Wang, Y. H.; Hu, C. W. *J. Chem. Soc., Dalton Trans.*, **2001**, 2, 121-129.
- S2** Sheldrick, G. M. *SHELXS97: Program for Crystal Structures Solution*; University of Göttingen: Göttingen, Germany, **1997**.
- S3** Sheldrick, G. M. *SHELXL-97: Program for Crystal Structures Refinement*; University of Göttingen: Göttingen, Germany, **1997**.
- S4** Brown, I. D.; Altermatt, D. *Acta Crystallogr.*, **1985**, B41, 244-247.
- S5** Thorp, H. H. *Inorg. Chem.*, **1992**, 31, 1585-1588.
- S6** O'Keeffe, M.; Brese, N. E. *Acta Crystallogr.*, **1992**, B48, 152-154.
- S7** Contant, R.; Thouvenot, R.; Dromzée, Y.; Proust, A.; Gouzerh, P. *J. Cluster. Sci.*, **2006**, 17, 317-331.
- S8** Rocchiccioli-Deltcheff, C.; Thouvenot, R. *Proc. 18th Colloq. Spectrosc. Int.* (Grenoble, France, **1975**), Vol. II, pp. 500.
- S9** Besecker, C. J.; Klemperer, W. G. *J. Am. Chem. Soc.*, **1980**, 102, 7598-7600.
- S10** Wang, J.; Duan, X.; Du, X.; Niu, J. *Cryst. Growth Des.*, **2006**, 6, 2266-2270.
- S11** Zhao, J.; Wang, J.; Zhao, J.; Ma, P.; Wang, J.; Niu, J. *Dalton Trans.*, **2012**, 41, 5832-5837.
- S12** Zhang, D.; Zhao, J.; Zhang, Y.; Ma, P.; Wang, J.; Niu, J. *Dalton Tran.*, **2013**, 42, 2696-2699.
- S13** Keita, B.; Mbomekalle, I. M.; Nadjjo, L. *Electrochem. Commun.*, **2003**, 5, 830-837.
- S14** Wang, X. L.; Kang, Z. H.; Wang, E. B.; Hu, C. W. *J. Electroanal. Chem.*, **2002**, 523, 142-149.